New Mechanical Features for Time-Domain WEC Modelling in *InWave*

David Ogden[*#1], Remy Pascal[*], Adrien Combourieu[**], David Forehand[φ], Lars Johanning[χ], Zhi-Ming Yuan[ψ]

[*]*Innosea Ltd., Edinburgh, UK*
[#]*Industrial Doctoral Centre for Offshore Renewable Energy (IDCORE)*
[1]email: david.ogden@innosea.fr
[**]*Innosea SAS, Nantes, France*
[φ]*Institute for Energy Systems, University of Edinburgh, Edinburgh, UK*
[χ]*College of Engineering, Mathematics and Physical Sciences, University of Exeter, Penryn, UK*
[ψ]*Department of Naval Architecture, Ocean and Marine Engineering, University of Strathclyde, Glasgow, UK*

Abstract- Numerical modelling of wave energy converters (WECs) can provide insights into device performance at an early stage and help de-risk projects before progressing to more advanced, costlier stages of development. Several software packages have been made available for this purpose in recent years. However, the lack of design convergence in the wave energy industry, with its wide range of working principles and mechanisms, means that many developers have been unable use these tools. Here we show that some limitations can be overcome by using an alternative multibody dynamics approach. A third party multibody dynamics code based on the Lagrange multiplier method, *Hotint*, has been coupled to *Innosea*'s existing WEC modelling code, *InWave*, and verified using existing test cases. This has made the modelling of many new types of mechanisms possible – include closed mechanical loops.

Keywords- *InWave*, Multibody Dynamics, WEC Simulation

I. INTRODUCTION

A well-known characteristic of the wave energy industry is the lack of design convergence among WECs. Indeed, despite the industry developing 8 different categories of WEC, all with distinct working principles, over a quarter of WEC concepts listed by EMEC in 2017 [1] are still classified as 'Other' (Figure 1). Some of these devices feature complex multibody mechanisms that are awkward to characterise.

In recent years several software tools have been developed specifically for multibody WEC modelling. However, they have so far focused on simple mechanisms typically comprised of rigid bodies connected by prismatic or revolute joints [2]–[5]. Hence, a WEC developer whose device contains more complex mechanisms might either have to devote resources to developing and verifying their own simulation tools, or perform no numerical modelling at all – potentially leading to sub-optimal designs and greater risks at more advanced stages of development.

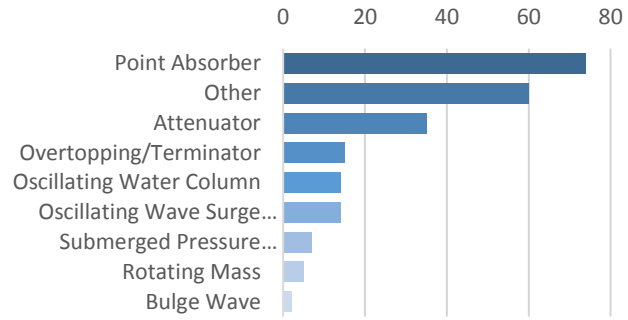

Figure 1. Classifications of 226 WECs listed by EMEC in 2017 [1].

Most WEC modelling tools (including *InWave*, *ProteusDS*, *WaveDyn*) have used *reduced-coordinate* multibody dynamics algorithms (aka general or relative coordinate methods; based on a set of ordinary differential equations (ODEs) derived from Lagrange's equations of the second kind) [4], [6]–[10]. These methods are known for their efficiency but not necessarily their versatility. Another multibody dynamics approach is the *Lagrange multiplier* method (aka redundant coordinate or constraint-based methods; based on a set of differential-algebraic equations (DAEs) derived from Lagrange's equations of the first kind). Lagrange multiplier methods are widely used across mechanical engineering and computer animation, as they enable a much wider range of constraints to be modelled and combined in a multibody system [11].

However, Lagrange multiplier methods have so far been less common in wave energy applications. Paparella presents a comparison of bespoke ODE and DAE multibody solvers [12] developed for hinged-barge models and Edwards et al. refer to a sequential impulse method used to model the *Albatern* device [13]. *WEC-Sim* utilizes a closed-source multibody dynamics algorithm included in *MATLAB* (*Simscape Multibody*) but the official *MATLAB* documentation does not explicitly describe the underlying theory.

In this paper, we show how a Lagrange multiplier multibody dynamics algorithm can help overcome some of the existing restrictions of multibody WEC modelling tools. A third party

multibody dynamics code based on the Lagrange multiplier method, *Hotint*, has been coupled to *Innosea's* existing multibody WEC modelling tool, *InWave*. To distinguish the new developments from the original *InWave* code, we refer to it as *InWave+H*. Verification of *InWave+H* is presented, and a demonstration of some of the new capabilities (e.g. closed mechanical loops) is also shown.

II. THEORY & METHODOLOGY

Here we present the underlying theory of the Lagrange multiplier method and show how it can incorporate fluid mechanics for WEC modelling. One of the main objectives of the Lagrange multiplier method is to determine the constraint force vector - $\boldsymbol{J}^T\vec{\lambda}$, and include it in the system's equations of motion:

$$\boldsymbol{M}\dot{\vec{u}} = \boldsymbol{J}^T\vec{\lambda} + \vec{f}_{ext}$$

Where $\vec{f}_{ext}$ contains all of the external forces acting on the system. For an n-body system,

$$\boldsymbol{M} = \begin{bmatrix} \boldsymbol{M}_1 & \boldsymbol{0} & \cdots & \boldsymbol{0} \\ \boldsymbol{0} & \boldsymbol{M}_2 & \cdots & \boldsymbol{0} \\ \vdots & \vdots & \ddots & \vdots \\ \boldsymbol{0} & \boldsymbol{0} & \cdots & \boldsymbol{M}_n \end{bmatrix}, \vec{u} = \begin{bmatrix} \vec{u}_1 \\ \vec{u}_2 \\ \vdots \\ \vec{u}_n \end{bmatrix}, \vec{f}_{ext} = \begin{bmatrix} \vec{f}_1 \\ \vec{f}_2 \\ \vdots \\ \vec{f}_n \end{bmatrix}$$

An important difference to reduced coordinate solvers is that the Lagrange multiplier method retains 6 degrees of freedom for each body, regardless of how it is constrained – hence each mass matrix ($\boldsymbol{M}_n$) has size 6×6, and the velocity and force vectors ($\vec{u}_n$ & $\vec{f}_n$) have size 6×1.

To represent a constraint in the system – for example, a ball joint – we can use a vector equation to define the positions on each body that are connected at the joint (Figure 2).

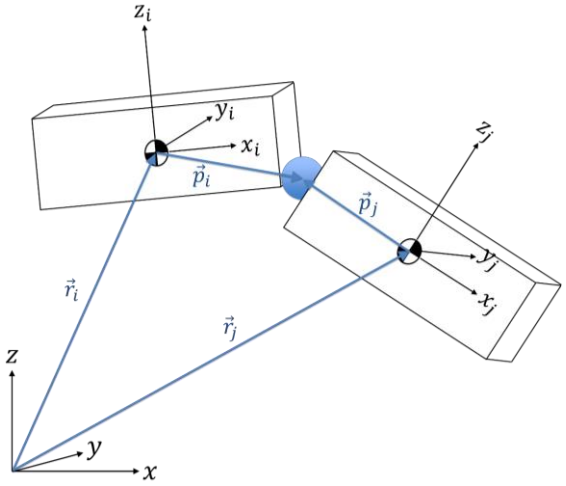

Figure 2. Constraint equation example: a ball joint.

$$\vec{0} = \vec{C}_k = (\vec{r}_i + \vec{p}_i) - (\vec{r}_j + \vec{p}_j)$$

$$\vec{0} = \vec{C}_k = \vec{r}_{pi} - \vec{r}_{pj}$$

Normally a system has to deal with several such constraints, hence a set of constraint equations can be combined in one vector, $\vec{C}$, and enforced at each time step. $\boldsymbol{J}$ is a Jacobian matrix, containing the partial derivatives of the constraint equations:

$$\boldsymbol{J} = \frac{\partial \vec{C}}{\partial \vec{s}} = \begin{bmatrix} \frac{\partial \vec{C}_1}{\partial \vec{s}_1} & \frac{\partial \vec{C}_1}{\partial \vec{s}_2} & \cdots & \frac{\partial \vec{C}_1}{\partial \vec{s}_n} \\ \frac{\partial \vec{C}_2}{\partial \vec{s}_1} & \frac{\partial \vec{C}_2}{\partial \vec{s}_2} & \cdots & \frac{\partial \vec{C}_2}{\partial \vec{s}_n} \\ \vdots & \vdots & \ddots & \vdots \\ \frac{\partial \vec{C}_n}{\partial \vec{s}_1} & \frac{\partial \vec{C}_n}{\partial \vec{s}_2} & \cdots & \frac{\partial \vec{C}_n}{\partial \vec{s}_n} \end{bmatrix}$$

Where $\vec{s}$ is the system's position vector. Hence, the Jacobian determines the directions of the constraint forces. $\vec{\lambda}$ is a vector of Lagrange multipliers, which determine the magnitudes of the constraint forces and must be solved for at each time step.

The equations of motion and the algebraic constraint equations can be combined to give the following system of differential—algebraic equations (DAEs):

$$\begin{bmatrix} \boldsymbol{M} & -\boldsymbol{J}^T \\ \boldsymbol{J} & \boldsymbol{0} \end{bmatrix} \begin{bmatrix} \dot{\vec{u}} \\ \vec{\lambda} \end{bmatrix} = \begin{bmatrix} \vec{f}_{ext} \\ \vec{f}_c \end{bmatrix}$$

Where $\vec{f}_c$ is the right hand side of the constraint equations. If the constraint equations are formulated on the position level, we refer to these as index-3 DAEs. Constraint equations formulated on the velocity level lead to index-2 DAEs, which are usually easier to integrate. Hence, a common solution method is to transform the position level constraint equations to the velocity level by differentiation. However, this approach of using 'constraint impulses' can lead to numerical drift – requiring additional stabilization routines or smaller time steps to compensate. *Hotint* uses high order (up to 20) implicit Runge-Kutta methods which allow the direct solution of both index-2 and index-3 DAEs [14].

The vector of external forces, $\vec{f}_{ext}$, is made up of all external forces acting on the system. In *InWave*, the hydrodynamic forces are based on linear potential flow theory.

$$\vec{f}_{ext} = -\vec{f}_{gravity} - \vec{f}_{hs} + \vec{f}_{ex} - \vec{f}_{rad} - \vec{f}_{pto}$$

Where,

$$\vec{f}_{hs} = \boldsymbol{C}_{hs}[\vec{s} - \vec{s}_{eq}]$$

$\boldsymbol{C}_{hs}$ is the matrix of hydrostatic restoring coefficients and $\vec{s}_{eq}$ is the position vector of the system at hydrostatic equilibrium.

For the wave excitation and radiation forces; $\vec{f}_{ex}$ and $\vec{f}_{rad}$, some pre-processing is required. *Nemoh* – a boundary element method (BEM) code [15] – is used to compute:

- Froude-Krylov force, $\vec{f}_{FK}(\omega)$

- Diffraction force, $\vec{f}_{diff}(\omega)$
- Added mass matrices, $\boldsymbol{A}(\omega)$
- Radiation damping matrices, $\boldsymbol{B}(\omega)$

We refer to these frequency-domain hydrodynamic coefficients collectively as the 'hydrodynamic database' (HDB). The wave excitation impulse response function (IRF), $\boldsymbol{K}_{ex}(\tau)$ can then be obtained by combining $\vec{f}_{FK}(\omega)$ and $\vec{f}_{diff}(\omega)$ and computing the following integral:

$$\boldsymbol{K}_{ex}(t) = \frac{1}{2\pi}\int_{-\infty}^{+\infty} \vec{f}_{ex}(\omega) e^{i\omega t} d\omega$$

$\vec{f}_{ex}(t)$ can then be computed by convolving the excitation impulse response with the wave elevation:

$$\vec{f}_{ex}(t) = \int_{-\infty}^{+\infty} \boldsymbol{K}_{ex}(\tau)\eta(t-\tau)d\tau$$

Similarly, the radiation impulse response function (RIRF), $\boldsymbol{K}_{rad}(t)$ and $\vec{f}_{rad}(t)$ can be obtained by computing the following integrals:

$$\boldsymbol{K}_{rad}(t) = \frac{2}{\pi}\int_{0}^{+\infty} \boldsymbol{B}(\omega)\cos\omega t \, d\omega$$

$$\vec{f}_{rad}(t) = \int_{0}^{t} \boldsymbol{K}_{rad}(t-\tau)\vec{u}(\tau)d\tau$$

The radiation force requires that the system's added mass at infinite frequency, $\boldsymbol{A}_\infty$, is added to the system's mass matrix:

$$(\boldsymbol{M} + \boldsymbol{A}_\infty)\dot{\vec{u}} = \boldsymbol{J}^T\vec{\lambda} + \vec{f}_{ext}$$

The inclusion of $\boldsymbol{A}_\infty$ can be difficult in some multibody dynamics codes. For example, *Chrono* [16] uses integration routines that do not assemble the entire system mass matrix, which prohibits the addition of the full infinite added mass matrix. Similarly, *Simscape Multibody* does not permit direct modification of the full system mass matrix. However, *Hotint* does permit access to the entire system's mass matrix, allowing $\boldsymbol{A}_\infty$ to be included directly. An overview of the *InWave+H* structure and process is shown in Figure 3. This coupling makes the following features available to be combined in a time-domain WEC model based on potential flow theory:

- 3D rigid bodies (6 dof)
- 3D point masses (3 dof – translations only)
- Coordinate constraints (position or velocity)
- Joints (spherical, revolute, prismatic, universal, sliding, cylindrical)
- Spring-dampers (linear and rotary)
- 3D rope elements
- Friction
- Closed kinematic loop mechanisms
- Arrays
- Controllers & TCP/IP communication for external control modules or co-simulation.

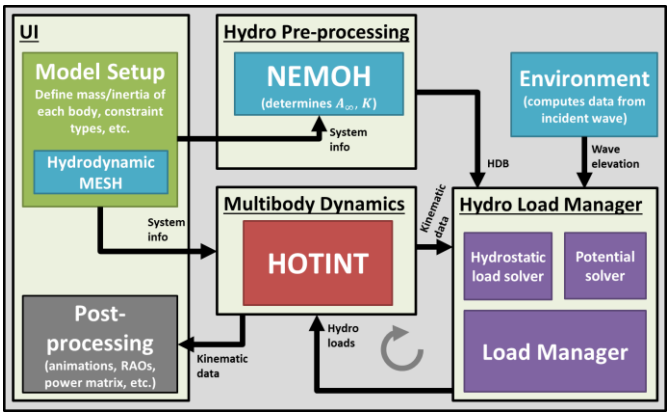

Figure 3. Overview of the structure of InWave+H. The coupling has been implemented in C++, with some pre/post-processing and automation routines in Python.

III. VERIFICATION

To verify the accuracy of *InWave+H*, existing *InWave* test cases were used. Some verification results for the F3OF model used in the WEC3 and NumWEC projects [2], [17] are presented.

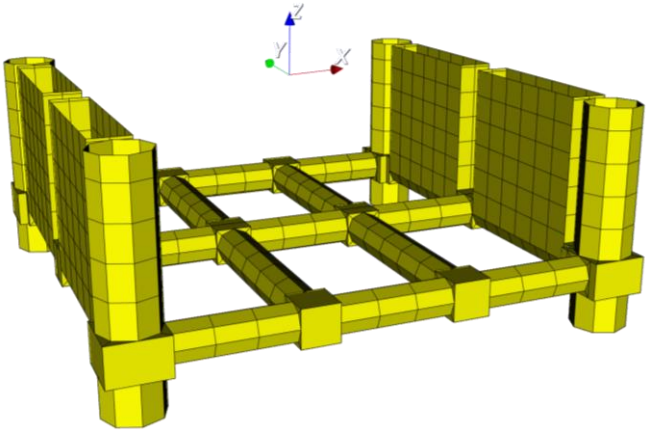

Figure 4. Hydrodynamic mesh of the F3OF model.

Parameter	Base	Flap 1	Flap 2
Mass (kg)	1089825	179250	179250
CoG – x (m)	0	-12.5	12.5
CoG – y (m)	0	0	0
CoG – z (m)	-9	-5.5	-5.5
Pitch inertia about body CoG $(kg \cdot m^2)$	76300000	1300000	1300000
Mooring stiffness (N/m)	100000	n/a	n/a

Table 1. Key Characteristics of the F3OF Model.

A useful decay test to check the model's hydrodynamic interactions is to give one flap a 10° displacement in still water, and let the radiated waves excite the other flap (Figure 5).

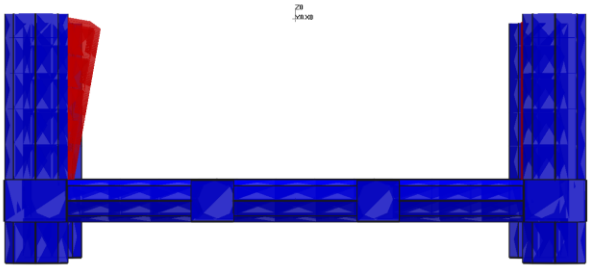

Figure 5. Decay test initial conditions: flap 1 given an initial offset of 10 degrees.

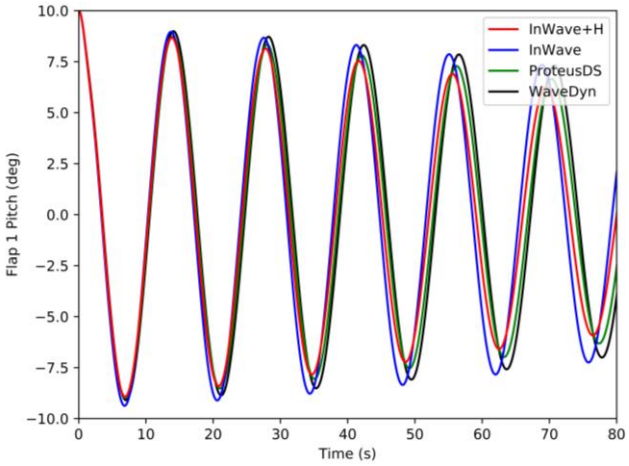

Figure 6. Flap 1 pitch angle - decay test results.

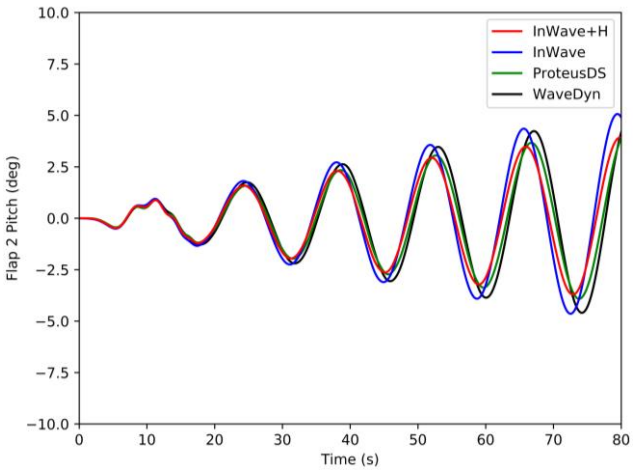

Figure 7. Flap 2 pitch angle - decay test results.

Figures 6 and 7 show some small discrepancies between the codes in both natural period and amplitude. This has been attributed to different methods being used to compute the HDB - future work will investigate these differences.

The model has also been verified for linear regular waves with amplitude 0.01m and periods from 5s to 15s with 1s intervals (Figure 8).

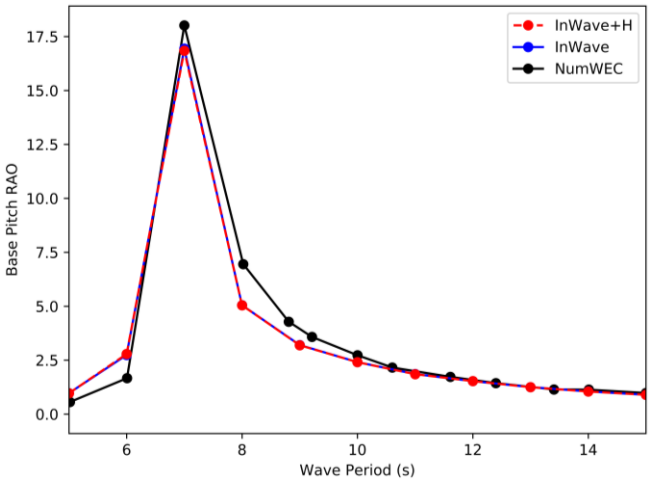

Figure 8. F3OF Base Pitch RAO Comparison.

Very good RAO agreement was observed with *InWave*. Some small discrepancies with NumWEC were observed, which is not fully understood but could possibly arise from slightly different hydrodynamic input settings (e.g. HDB frequency step size ($d\omega$) or RIRF length (t_{IRF})).

IV. APPLICATIONS

To demonstrate some of the new features that are available in *InWave+H*, we present two models based on the 'Squid' and 'Hex' models shown by McDonald et al. [18] and Barker-Ewart et al. [19] (Figure 9). These models consist of a number of nodes connected by link arms, with power being extracted from the relative motion between the nodes and the link arms. We refer to the single device as '4N3LA' (4 nodes, 3 link arms) and the array of connected devices as '9N9LA' (9 nodes, 9 link arms).

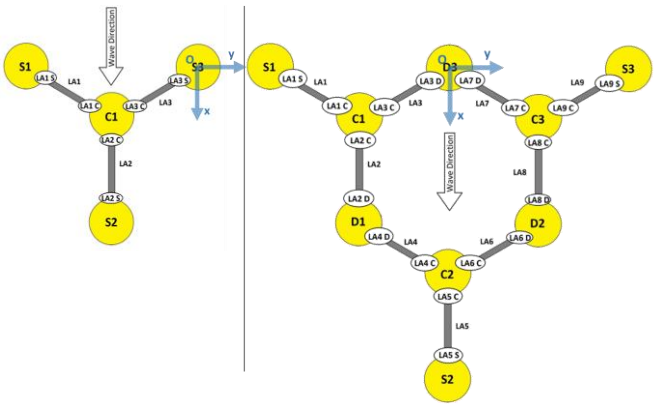

Figure 9. Labelling system for Squid & 4N3LA (left) and Hex & 9N9LA (right) – plan views [18].

For numerical modelling purposes, the hydrodynamic forces on the link-arms have been assumed to be negligible, hence the HDB is computed for the nodes only. The estimated dimensions for one node are shown in Figure 10. By estimating a link arm length of 1.4m, the positions of each node in the system can then be determined by trigonometry (Table 2).

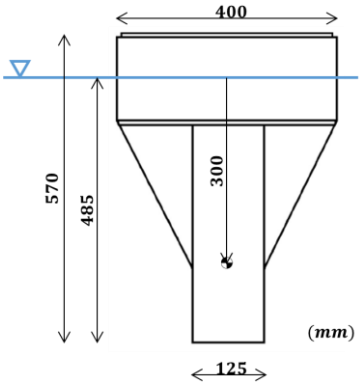

Figure 10. Estimated node dimensions used in the 4N3LA and 9N9LA models.

Node	CoG -x (m)	CoG – y (m)	CoG – z (m)
S3	0	0	-0.3
C1	0.7	-1.21	-0.3
S1	0	-2.42	-0.3
S2	2.1	-1.21	-0.3

Table 2. 4N3LA - Node Positions used in the 4N3LA and 9N9LA models.

Based on the estimates shown in Figure 10 and Table 2, the hydrodynamic mesh was created (Figure 11) and the HDB computed with *Nemoh*.

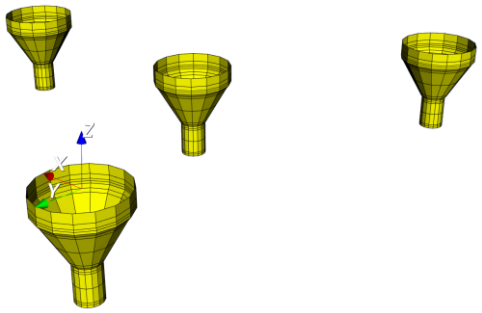

Figure 11. 4N3LA mesh.

The link arms are then included in the mechanical model, with their centre of gravity at a depth of 0.4m. They are assumed to be neutrally buoyant. Between each link arm and node, there is a power take-off (PTO) absorbing power from the relative pitch and yaw degrees of freedom. To model this, we combined two constraint types: firstly, a Lagrange multiplier constraint takes care of the spherical joint kinematics by using a vector constraint equation to ensure that the designated points on each body are exactly co-located, but can rotate freely. Secondly, a penalty constraint applies angular stiffness and damping torques to the relative pitch and yaw motion between the bodies (Figure 12). The penalty constraint permits different PTO stiffness and damping settings to be used (K_{PTO} and C_{PTO}) in the model, and from the damping torque we can estimate the power produced.

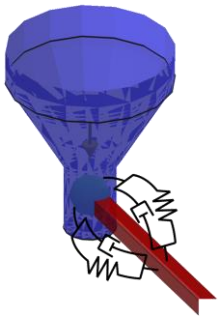

Figure 12. Schematic of the relative pitch & yaw PTOs applied between each node and link arm.

3D rope elements were used to model the mooring system, with rope connection points included as 3D mass elements (Figure 13).

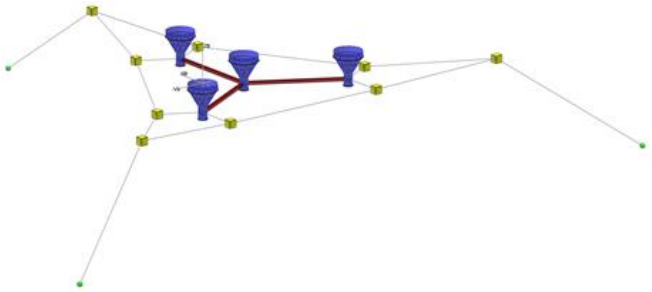

Figure 13. Overview of the time-domain model in Hotint GUI.

The stability of the system has been checked by observing the system's response in small amplitude regular waves (Figure 14).

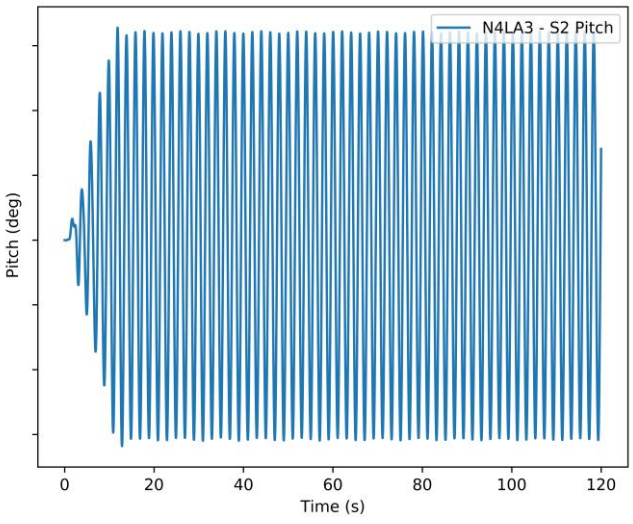

Figure 14. Pitch angle of the 4N3LA rear node (S2) for regular waves.

The model's power output can be obtained by multiplying the penalty constraint's damping torque by the relevant angular velocity (either relative pitch or relative yaw between node and link arm). These individual PTO power outputs can be

combined to determine the system's total power output – as shown in Figure 15 for irregular waves.

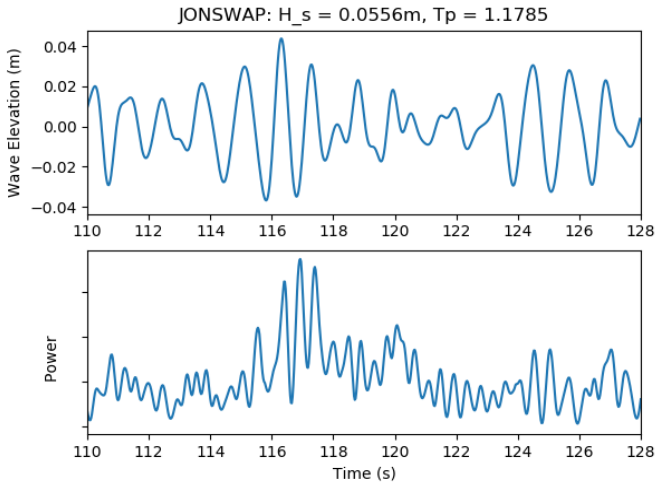

Figure 15. Time series for irregular wave elevation (top) and total system power output (bottom).

The 4N3LA model can easily be expanded to model the larger array, 9N9LA – where 6 of the rigid bodies form a hexagonal closed kinematic loop in the middle of the device (Figures 16 and 17).

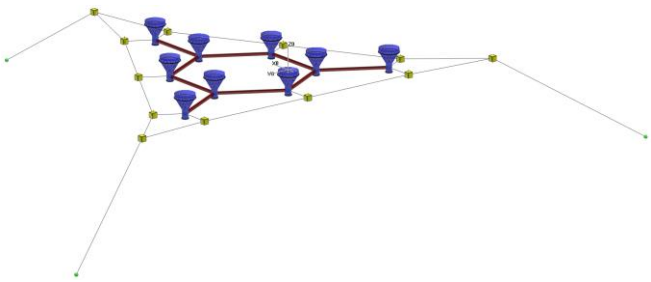

Figure 16. 9N9LA model in Hotint GUI.

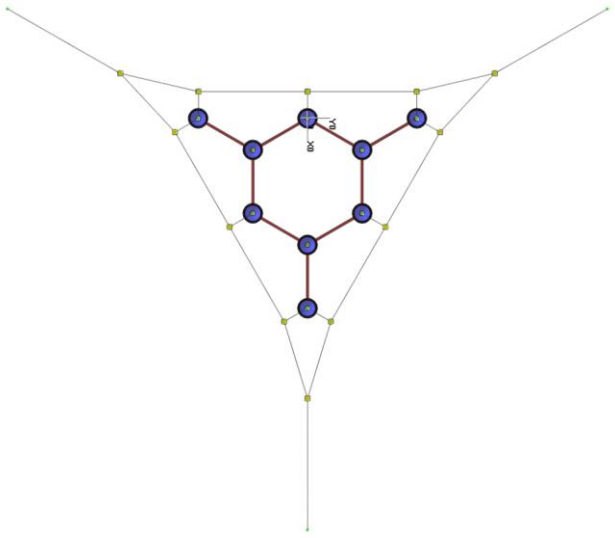

Figure 17. Plan view of the 9N9LA model.

To explore the effect of mechanical coupling in 9N9LA, RAOs of the nodes S2 and D1 pitching relative to the link-arms LA5 and LA2 can be compared with the rear node of the 4N3LA (S2) pitching relative to the link arm LA2 [18]. For baseline PTO setting, we selected stiffness and damping coefficients that would give similar efforts to the hydrostatic stiffness and radiation damping forces. Parametric variation has been performed around these base values to compare the effects of PTO stiffness and damping parameters on the RAOs (Figure 18).

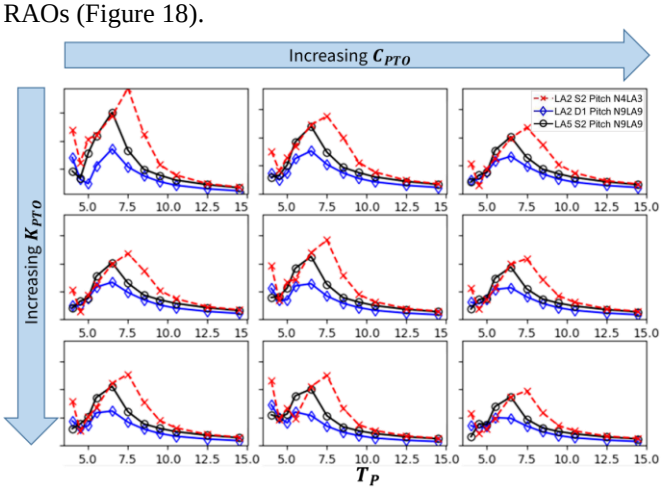

Figure 18. RAO comparison for parametric variation of PTO stiffness and damping parameters.

Using this approach it is possible to explore the effect that mechanical coupling, with different PTO settings, has on the overall performance of the device.

V. CONCLUSION

A multibody dynamics solver (*Hotint*) based on the Lagrange multiplier method has been utilized for wave energy applications. In constrast to reduced-coordinate multibody algorithms, this approach can give WEC designers greater freedom over the types of mechanisms that can be included in a numerical model. Constraints can be combined in order to get more accurate representations of complex mechanisms, which can be critical in WEC modelling. This approach requires a greater number of hydrodynamic coefficients to be computed, which may impact performance compared to reduced-coordinate methods. Future work will focus on comparing the performance of both approaches and experimental validation.

ACKNOWLEDGMENT

The authors would like to thank the Energy Technology Institute and the Research Council UK Energy Programme for funding this research as part of the IDCORE programme (EP/J500847/1). Sincere thanks are also given to Maxime Philippe (formerly of *Innosea SAS*), Anthony McDonald (formerly of *Albatern Ltd.*) and the *Hotint* support team.

REFERENCES

[1] EMEC, "Wave developers," 2017. [Online]. Available: http://www.emec.org.uk/marine-energy/wave-developers/.

[2] A. Combourieu, M. Lawson, A. Babarit, K. Ruehl, A. Roy, R. Costello, P. L. Weywada, and H. Bailey, "WEC3 : Wave Energy Converter Code Comparison Project," in *Proceedings of the 11th European Wave and Tidal Conference EWTEC 2015*, 2015.

[3] F. Wendt, Y. Yu, K. Nielsen, K. Ruehl, T. Bunnik, I. Touzon, B. W. Nam, J. S. Kim, K. Kim, C. E. Janson, K. Jakobsen, S. Crowley, L. Vega, K. Rajagopalan, T. Mathai, D. Greaves, E. Ransley, P. Lamont-kane, W. Sheng, R. Costello, B. Kennedy, S. Thomas, P. Heras, H. Bingham, A. Kurniawan, M. M. Kramer, D. Ogden, S. Girardin, P. Wuillaume, D. Steinke, S. Beatty, P. Schofield, J. Jansson, and J. Hoffman, "International Energy Agency Ocean Energy Systems Task 10 Wave Energy Converter Modeling Verification and Validation," in *Proceedings of the 12th European Wave and Tidal Conference, EWTEC 2017*, 2017, pp. 1197--1–10.

[4] J. Cruz, E. Mackay, M. Livingstone, and B. Child, "Validation of Design and Planning Tools for Wave Energy Converters (WECs)," in *1st Marine Energy Technology Symposium METS13*, 2013.

[5] M. Lawson, Y. Yu, K. Ruehl, and C. Michelen, "Improving and Validating the WEC-Sim Wave Energy Converter Modeling Code," *Proc. 3rd Mar. Energy Technol. Symp. METS2015*, no. April, 2015.

[6] A. Combourieu, M. Philippe, F. Rongère, and A. Babarit, "InWave : A New Flexible Design Tool Dedicated to Wave Energy Converters," in *ASME 2014 33rd International Conference on Ocean, Offshore and Arctic Engineering, OMAE2014*, 2014.

[7] J. Lucas, M. Livingstone, M. Vuorinen, and J. Cruz, "Development of a wave energy converter (WEC) design tool - application to the WaveRoller WEC including validation of numerical estimates," in *Proceedings of the 4th International Conference on Ocean Energy, ICOE 2012*, 2012.

[8] R. S. Nicoll, C. F. Wood, and A. R. Roy, "Comparison of Physical Model Tests With a Time Domain Simulation Model of a Wave Energy Converter," in *Proceedings of the ASME 2012 31st International Conference on Ocean, Offshore and Arctic Engineering*, 2012.

[9] M. Ó'Catháin, B. J. Leira, J. V. Ringwood, and J. C. Gilloteaux, "A modelling methodology for multi-body systems with application to wave-energy devices," *Ocean Eng.*, vol. 35, no. 13, pp. 1381–1387, 2008.

[10] F. Rongère and A. H. Clément, "Systematic dynamic modeling and simulation of multibody offshore structures: Application to wave energy converters," in *ASME 2013 32nd International Conference on Ocean, Offshore and Arctic Engineering*, 2013.

[11] D. Baraff, "Linear-Time Dynamics using Lagrange Multipliers," in *Computer Graphics Proceedings, Annual Conference Series (SIGGRAPH 96)*, 1996, pp. 137–146.

[12] F. Paparella, "Modeling and Control of a Multibody Hinge-Barge Wave Energy Converter," Maynooth University, 2017.

[13] W. Edwards, D. Findlay, D. Scott, and P. Graham, "SHAPE Pilot Albatern: Numerical Simulation of Extremely Large Interconnected Wavenet Arrays," 2014.

[14] J. Gerstmayr, "Hotint – A C++ Environment for the Simulation of Multibody Dynamics Systems and Finite Elements," in *Multibody Dynamics 2009, ECCOMAS Thematic Conference*, 2009, no. July, pp. 1–20.

[15] A. Babarit and G. Delhommeau, "Theoretical and numerical aspects of the open source BEM solver NEMOH," in *Proceedings of the 11th European Wave and Tidal Energy Conference.*, 2015, pp. 1–12.

[16] H. Mazhar, T. Heyn, A. Pazouki, D. Melanz, A. Seidl, A. Bartholomew, A. Tasora, and D. Negrut, "Chrono: a parallel multi-physics library for rigid-body, flexible-body, and fluid dynamics," *Mech. Sci*, vol. 4, no. 1, pp. 49–64, 2013.

[17] A. Babarit, J. Hals, A. Kurniawan, M. Muliawan, T. Moan, and J. Krokstad, "The NumWEC project," 2011.

[18] A. McDonald, Q. Xiao, D. Forehand, and D. Findlay, "Experimental Investigation of Array Effects for a Mechanically Coupled WEC Array," in *Proceedings of the Twelfth European Wave and Tidal Energy Conference*, 2017, pp. 929–1--9.

[19] L. Barker-Ewart, P. R. Thies, T. Stratford, and N. Barltrop, "Optimising structural loading and power production for floating wave energy converters," in *Proceedings of the Twelfth European Wave and Tidal Energy Conference*, 2017, pp. 840–1--10.